International Journal of Solids and Structures 301 (2024) 112946

Contents lists available at ScienceDirect

International Journal of Solids and Structures

journal homepage: www.elsevier.com/locate/ijsolstr

A machine learning assisted multifidelity modelling methodology to predict 3D stresses in the vicinity of design features in composite structures

Omar A.I. Azeem *, Silvestre T. Pinho

Department of Aeronautics, Imperial College London, Exhibition Road, London SW7 2AZ, UK

ARTICLE INFO

Keywords:
Machine learning
Finite element analysis
Multifidelity
Global-local submodelling
Predictive virtual testing

ABSTRACT

Multifidelity global–local finite element (FE) analyses are typically used to predict damage initiation hotspots around repetitive design features in large composite structures, such as composite airframes. We propose the use of machine learning (ML) methods to accelerate these analyses. We demonstrate this ML assisted framework for the stress analysis of a hole in plate feature in an aerospace C-spar structure. To enable this framework, we develop the following original features: a computationally efficient sampling scheme; a work-equivalent boundary condition homogenisation scheme; a volume averaged ply-by-ply stress approach; and a sequential long-short term memory neural network reformulated from a time basis to a stacking sequence basis with further bi-directionality customisation. Overall, we show that the developed method results in high-accuracy prediction of 3D stresses, with over two orders of magnitude reduction in modelling and simulation time compared to FE analyses.

1. Introduction and literature review

High-fidelity computational methods are necessary for accurate stress analysis and consequent damage and failure modelling during predictive virtual testing of composite structures. However, these methods are typically unfeasible to carry out across large composite structures. Therefore, the current design process often consists of multifidelity and multiscale finite element (FE) submodelling analyses to predict damage initiation hotspots around features of interest such as bolted joints, ply drops and ply cuts (Ostergaard et al., 2011).

Such analyses use low-fidelity macroscale global model simulations to screen highly stressed areas and to determine the field displacements that drive progressively higher fidelity mesoscale local models around features of interest. However, this design process remains slow, repetitive and expert-dependent, as there may be thousands of such features.

The use of machine learning (ML) within this workflow may help address these problems, as large amounts of expert-gathered data from previous simulations can be recycled to create surrogate models that faster predict stresses around these repetitive features of interest. This will contribute to a step-reduction in the development cycle of airframes, as desired to effectively meet increasing aircraft demand (Global Market Forecast|Airbus, 2023) and the call for sustainable aviation (IATA - Fly Net Zero, 2023).

Note that in addition to the uncoupled submodelling procedure whereby local models run sequentially after the global models, there exists strongly coupled submodelling (Krueger and O'Brien, 2001) whereby the local models run parallel to the global models. There also exists loosely coupled submodelling (Akterskaia et al., 2019) whereby analyses are performed sequentially but information between global and local is exchanged in a two-way approach until model convergence. However, the uncoupled submodelling framework lends itself towards machine learning as a separate library of feature submodels for training data can be used to continuously train the machine learning model by high performance computers offline.

Fast and efficient multiscale methods that do not employ ML have been developed (SwiftComp for Efficient Modeling of Composites|AnalySwift, 2023). However, they act uniformly as a material definition and are based upon simple periodic boundary conditions. Therefore, they are not applied for localised features with more complex boundary conditions variations. To accelerate uncoupled submodelling around localised features, without the use of ML, the Carrera Unified Formulation can be used to generate a 2D or 1D local model as opposed to a 3D local model (Nagaraj et al., 2021). Another study predicts the behaviour of design features given varying local boundary conditions, but of fixed laminate stacking sequence and feature geometry (Zou et al., 2021). Varying these additional factors results in a highly dimensional and non-linear

* Corresponding author.
E-mail address: oai15@imperial.ac.uk (O.A.I. Azeem).

https://doi.org/10.1016/j.ijsolstr.2024.112946
Received 1 January 2024; Received in revised form 21 May 2024; Accepted 23 June 2024
Available online 24 June 2024

problem, which ML can be used to address.

ML has been used to develop microscale surrogates in multiscale analyses via the prediction of constitutive relationships (Logarzo et al., 2021) and via domain decomposition methods (Krokos et al., 2022). Data driven methods have been used to accelerate concurrent multiscale FE2 analyses by prediction of nested microscale model behaviour (Le et al., 2015) and in a scale decoupled framework by searching stress–-strain pairs in a material genome database (Xu, 2020). A data-driven method for coupled global–local analyses of localised features such as spot welds has been developed to improve global model stiffness behaviour (Reille, 2021); however, this method doesn't provide details of the ply-by-ply mesoscale stresses required to predict damage initiation for composite structures. Thus, the use of ML to predict high-fidelity 3D stresses around mesoscale features in uncoupled global local submodelling has not been previously achieved in open literature.

This use of ML requires the creation of surrogate mesoscale models that capture the effect of varying laminate stacking sequence, feature geometry and boundary conditions in an optimised manner, to minimise the training dataset size. This therefore leads to further challenges that are resolved in this work:

- Surrogate models that vary laminate stacking sequences sample from either the ply angle space (defined as the number of plies in each angle and the number of plies in total) or the lamination parameters space (which are derived from the 'ABD' stiffness matrix) (Fan et al., 2023). A good distribution of samples in one space does not guarantee good distribution in the other space. Furthermore, for the laminate parameter space, the stacking sequence must be reverse calculated using computationally expensive genetic algorithms. Therefore, we require a low computational cost design of experiment that samples laminates which are well distributed in both ply angle and lamination parameter spaces.
- Surrogate models that capture the effect of boundary conditions are limited to simple uniaxial or biaxial variations of boundary loading (Le et al., 2015; Sun et al., 2021). However, for our problem, it is required to understand the effect of complex loading vectors around the local submodel boundary. The nodes on this boundary may change in number and location depending on the size of the local model and the meshing strategy. Therefore, boundary conditions must be simplified, and mesh dependency must be alleviated, to make the problem have a feasible dimensionality and a reduced, fixed training dataset input size.

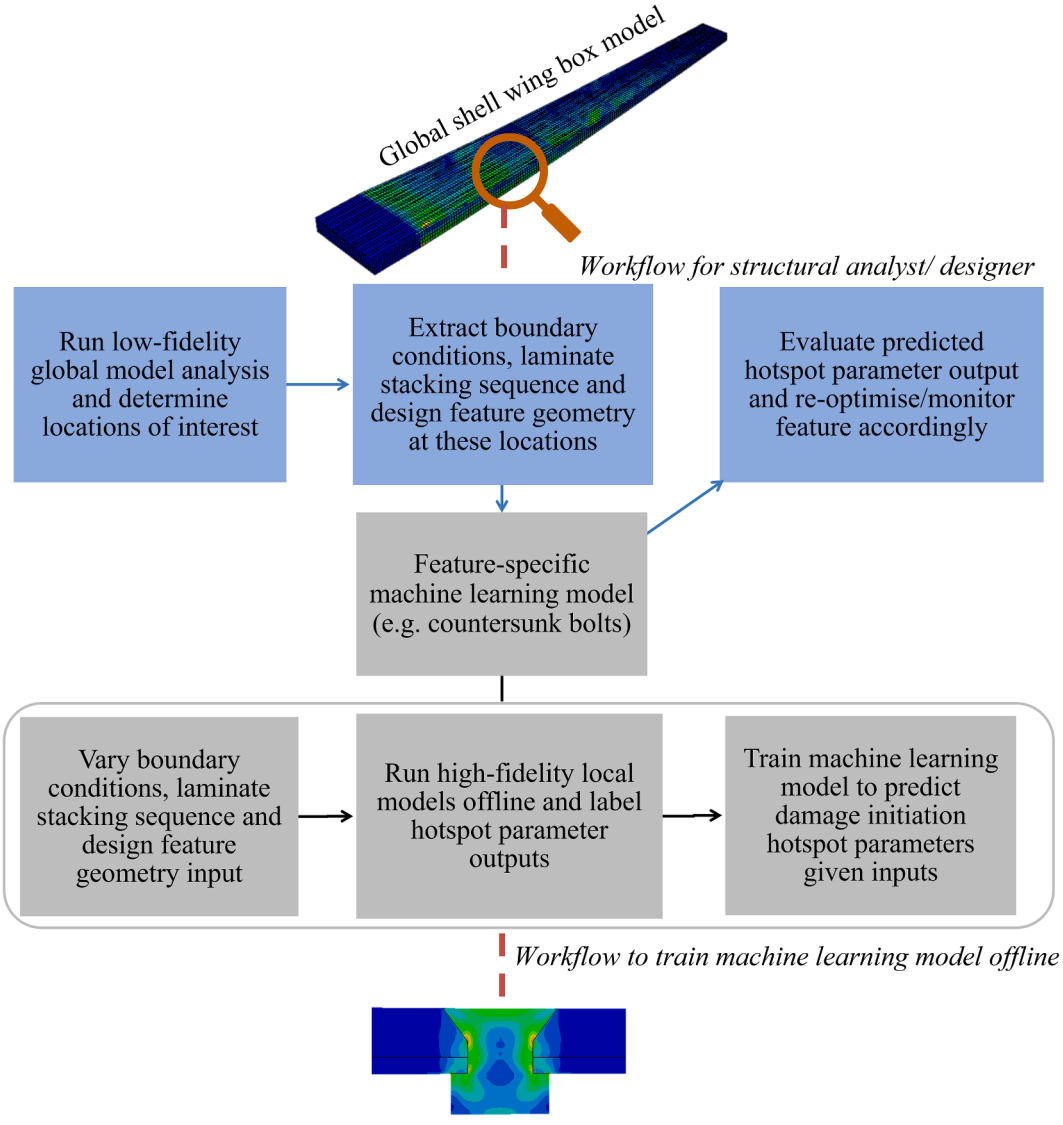

Fig. 1. Envisioned workflow for machine learning assisted global–local submodelling during airframe design, with a bolted joint as an example.

- In a similar manner, the nodal stresses that must be predicted in the local model may change in number and location depending on the size of the local model and the meshing strategy. Therefore, the 3D stresses must be simplified, and mesh dependency must be alleviated, to make the problem have a feasible dimensionality and a reduced, fixed training dataset output size.
- Furthermore, our problem must be formulated into a feasible ML problem and an appropriate hypertuned neural network must be selected.

To meet these challenges, we investigated: improved sampling; feature engineering of model inputs with a boundary condition homogenisation scheme; feature engineering of model outputs with a non-local stress analysis approach; and selection of suitable ML networks.

Ultimately, the envisioned workflow (see Fig. 1) aims to accelerate virtual testing with a ML surrogate that is trained offline on feature-specific high-fidelity local models. We demonstrate this workflow for the stress analysis of hole in plate features on a composite C-spar structure.

2. Methodology

2.1. Workflow

The workflow for this new methodology is divided into two parts as shown in Fig. 2. The first workflow (A) is used to develop the machine learning model to predict 3D stresses in the high-fidelity local model. In the second workflow (B), we interrogate boundary conditions in the region of interest of the low-fidelity global model and use our machine learning model to predict 3D stresses of a local feature in this region. We use Abaqus/2021 (Dassault Systemes, 2023) to generate our FE models. We use TensorFlow (Abadi, et al., 2016) and Keras (Chollet, Dec. 15, 2023.) to develop our ML models.

To begin the first workflow, we use a package in RStudio (RStudio Team, 2020) to generate the design of experiment, which is post-processed using Python and saved as csv files. Python scripting is then used to generate homogenized medium-fidelity intermediate models with varying boundary conditions which drive high-fidelity local models with varying hole geometry and laminate stacking sequences. Details of the fidelities used, and the homogenisation process are given in section 2.2.2. Simulations are run in parallel on a remote HPC cluster and further python scripting is used to extract and post-process the 3D stresses of interest. This data is saved in csv files. Machine learning models are developed using TensorFlow and Keras and the best-performing networks are saved. This workflow can be run offline, and a library of machine learning models for different design features can be generated ready for use. In this study the design feature of interest used as a generic and representative example is an open hole.

To use these developed machine learning models in the second workflow online i.e., in the design phase, we first interrogate the boundary conditions in the region of interest of the low-fidelity global model. In this study the global structure of interest is a C-spar. The boundary conditions are homogenized using a python script and combined with the details of the laminate stacking sequence and hole geometry in the region of interest as input to the machine learning model. Fast 3D through thickness predictions in the region of interest then follow, which can be visualized and post-processed as desired.

2.2. Machine learning modelling pipeline

2.2.1. Design of experiment

We generate a maximum projection Latin hypercube sampling (LHS) set of 150 samples across at least 4 dimensions. Four dimensions belong to the ply angle space, i.e., percentage of plies in 0°,+45° and 90° directions and total number of plies. The remaining dimensions represent the parameters required to represent feature geometry. For design features such as bolted joints, which may be represented by multiple geometry parameters, it is important to use a non-dimensional sampling method such as LHS. The maximum projection variant maximises the space-filling properties of LHS on projections to all subsets of factors (Joseph et al., 2015).

The percentages of plies in each direction are not independent variables. To conserve the space-filling properties of our sampling method, we transform the sampling space to satisfy our feasibility region and resultant probability distributions. This is achieved by rescaling the decimal values representing the ply angle percentages to ensure that their sum is unity. The sampling distribution for the variables in this study are shown in Fig. 3.

We then generate 1000 feasible laminates for each sample. Composite design guidelines (Niu, 1992) are encoded, ensuring that laminates are: symmetric, balanced, having at least 10 % of plies in each direction, with + 45° surface plies, and no more than 4 consecutive plies in the same angle. For each laminate, we calculate lamination parameters as (Albazzan et al., 2019):

$$L_1 = \int_{1/2}^{1/2} (cos2\theta) d\bar{z}$$

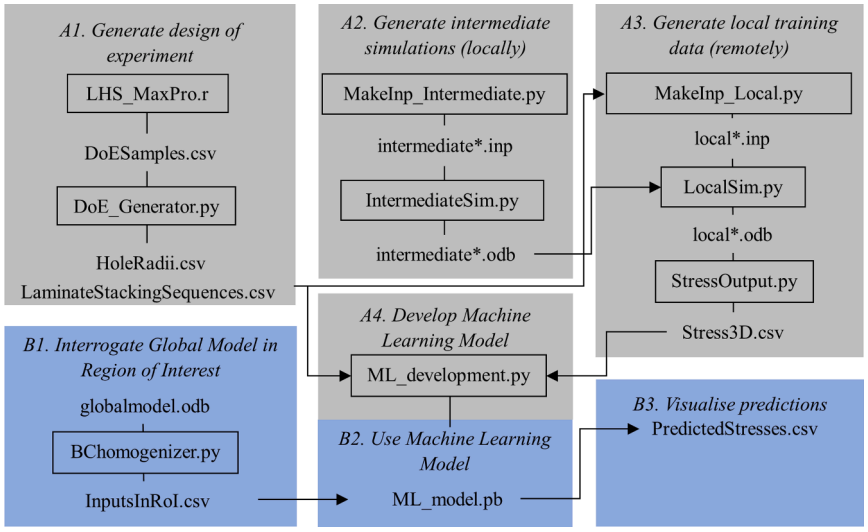

Fig. 2. Code workflow for open hole proof of concept. * indicates files are created for each laminate.

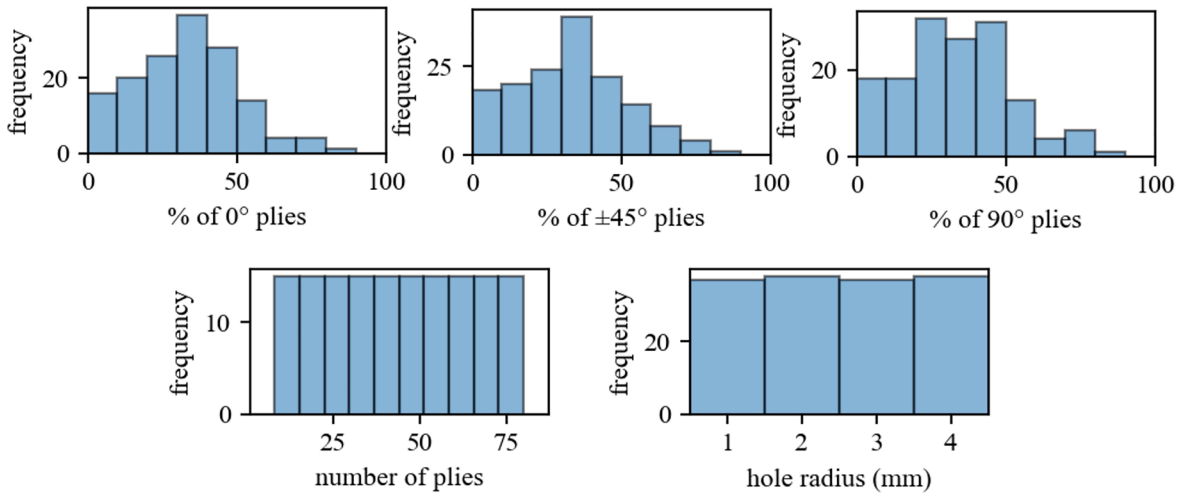

Fig. 3. Sampling set distribution.

$$L_2 = \int_{1/2}^{1/2} (cos4\theta) d\bar{z}$$

$$L_3 = 12 \int_{1/2}^{1/2} \bar{z}^2 (cos2\theta) d\bar{z}$$

$$L_4 = 12 \int_{1/2}^{1/2} \bar{z}^2 (cos4\theta) d\bar{z}$$

Using a maximin criterion we finally choose the feasible laminate for each sample which maximises the average Euclidean distance of samples in the lamination parameter space.

2.2.2. *Feature engineering input*

As our models are linear elastic, we can make use of the principle of linear superposition. We can apply a unit displacement to each boundary nodal degree of freedom independently, holding other degrees of freedom fixed, and save the resulting stress distributions for the local model. Then, for a given set of boundary displacements, we can scale the unit displacements and superimpose the resulting independent stress distributions.

To reduce the total nodal degrees of freedom, we can use Abaqus' in-built submodelling routine. We derive an intermediate shell model which is 2D and has a higher mesh size than the global model and therefore a fewer and fixed number of boundary nodes. This workflow is visualized in Fig. 4(a).

However, when interrogating the global model during design, the boundary nodes of the intermediate mesh may not align with the corresponding nodes in the global mesh. Therefore, the in-built Abaqus interpolation would result in non-equivalent work along each boundary. To account for this, a work-equivalent boundary condition homogenisation step is proposed.

This homogenisation requires the detailed boundary condition variation as input. This is obtained using Abaqus' in-built interpolation, to drive an intermediate model with higher mesh density. We conserve the displacement at the vertices and the net displacement along each boundary edge for each degree of freedom. This is done by integrating the displacement by each boundary in each degree of freedom and ensuring that the interpolated displacements are scaled so their integration results in an equivalent value. Assuming constant stiffness of the intermediate model along each boundary edge, this results in loading each edge with equivalent work. According to St. Venant's principle, this will result in equivalent stress developing a sufficient distance from the boundary. Fig. 4(b) demonstrates this alternative submodelling workflow.

In section 3.2 we investigate the effect of the order of boundary nodal degree of freedom reduction and the effect of hole proximity to the boundary on stress errors and the distance from the loaded edge to which stresses converge. We compare the effect of direct interpolation and work-equivalent homogenisation during this study.

The local solid models used to gather training data are in a different coordinate system to the intermediate models, that are positioned in the area of interest in the global model. A boundary condition transformation is therefore needed. The error of our ML model in predicting stress response is scaled by the magnitude of the total displacement for a given degree of freedom. Therefore, a requirement is that this

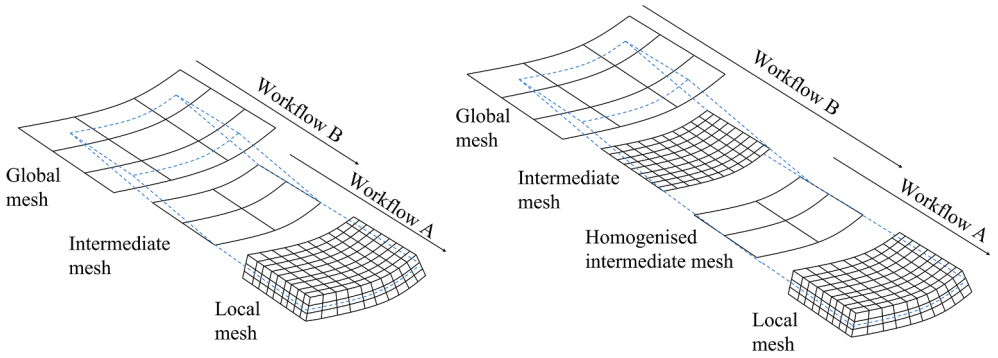

(a) In-built interpolation only (b) Work-equivalent homogenisation

Fig. 4. Global-local submodelling configurations.

transformation results in minimum values of nodal displacements. This requires us to remove any free body motion. To achieve this, we project the intermediate shell onto a plane of its best fit, then determine the distance of boundary nodes to their projected positions to determine the transformed displacements (see Fig. 5).

2.2.3. Feature engineering output

For open hole features and bolted joints, the point stress or the average stress a given distance ahead of the hole boundary is often used to predict failure (Whitney and Nuismer, 1974). We adopt a similar non-local approach in our study:

$$\overline{\sigma}_j = \frac{\sum_{e=1}^{n} \sigma_{j,e} * V_e}{\sum_{e=1}^{n} V_e}, \text{for j in } \{11, 22, 33, 12, 13, 23\}$$

where we obtain the volume averaged stress for a given stress component $\overline{\sigma}_j$, by averaging the 3D stress components of elements 'e' within a volume bounded by the ply thickness and a given distance to the feature boundary.

This volume averaging allows us to remove mesh dependence and to predict a low, fixed number of output stresses. In section 3.3 we investigate the use of volume averaged stresses and the selection of appropriate distance to feature boundary to volume average over.

2.2.4. Neural network selection

Our input data consists of the laminate stacking sequence and feature geometry. We represent the laminate stacking sequence as the explicit sequence of ordered ply angles. Feature geometry is transformed to a fixed value sequence and added as further dimensions to the input data. Our output data consists of a sequence of ply-by-ply volume averaged stress components. We train 6 ML models to each predict a given stress component when loading a given laminate by n degrees of freedom at the boundary, see Fig. 6.

As both our input and output data result in a sequence-to-sequence problem, we use sequential neural networks. Sequential neural networks are commonly used to predict time series, in applications such as financial modelling (Géron, 2019). However, in this study, we reformulate the application of sequential networks to a layup stacking sequence basis, as opposed to a time basis. For the neural network, input and output sequences must be the same length across different laminates, therefore we use zero padding to achieve this.

Recurrent neural networks (RNNs) are typically the simplest example of such networks. For our problem, stress predictions will be related to the laminate stiffness. In classical laminate theory, this stiffness is calculated by considering all the plies in the laminate simultaneously. Therefore, long-range effects in the sequence are of importance. For such sequences, RNNs may suffer a vanishing gradient problem and therefore a long-short term memory (LSTM) neural network is typically used to address these concerns. Consideration of the sequence in the forward and backwards direction may be useful for our problem as our laminates are symmetric. This can be done by adding a bidirectionality wrapper to the neural network.

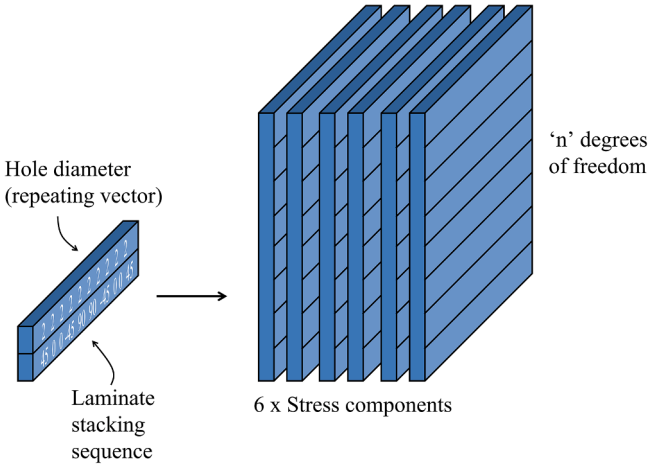

Fig. 6. Network input and outputs.

Further improvements to prediction accuracy may be achieved by stacking these neural networks to increase the network depth and using neural dropout, whereby neurons are frozen during training to allow the network to learn patterns in a more robust manner (Géron, 2019). These techniques can be used to address overfitting, whereby the model struggles to generalize to test data not seen during training.

Adam optimiser is used to implement stochastic gradient descent to update weights in the model. Loss is calculated using mean square error to penalize large errors, and the error metric is given as mean absolute error. The models are run to 10 000 epochs or until the model stops learning using early stopping.

We hold 10 % of samples for the test set. K-fold cross-validation is used to partition the remaining samples into training and validation data. K-fold cross-validation allows us to repeat test a given model's performance and therefore derive a mean prediction error. Three folds are used for nominal testing, resulting in a training:validation:test ratio of 60:30:10.

2.3. Finite element modelling methodology

A low-fidelity global model of a C-spar is generated to determine realistic boundary conditions in potential regions of interest. In the event of bolt failure, an open hole situated in the flanges of the C-spar may constitute a worst-case scenario. This global model will allow the comparison of stresses of local open hole models simulated via FE sub-modelling methods and those simulated via ML surrogate methods.

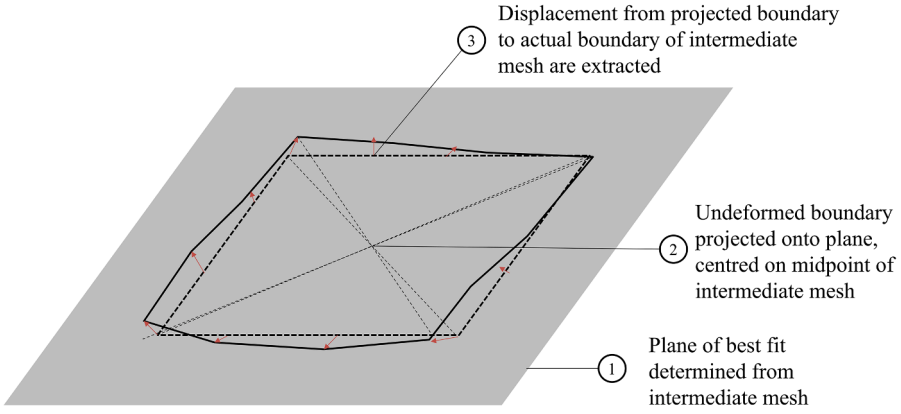

Fig. 5. Global-local coordinate transformation method.

Models are linear-elastic, and the analyses are implicit as typical in a design stage (Ostergaard et al., 2011). We use IM7/8552 carbon fibre epoxy prepreg, whose ply properties are given in Table 1. Each ply has a thickness of 0.125 mm.

Coarse conventional shell elements (S4R), as typically used in global airframe models (Ostergaard et al., 2011), with a mesh size of 10 mm are used to model the low-fidelity C-spar structure. The C-spar is sized based on the geometry of a small business jet (Cessna Citation Mustang Dimensions – FlyRadius, 2023). Quasi-isotropic layups are assigned via the composite layup feature in Abaqus. Laminate thicknesses vary in between 1–10 mm. This range represents laminate thickness at the root of the wingbox and towards the tip. One end of the structure is fully constrained in all degrees of freedom. The opposite end is coupled to a reference node with a force applied to result in beam bending. The magnitude of this applied force is chosen to result in a maximum in-plane strain of the laminate within a design allowable of 4500 microstrains (Creemers et al., 2009).

The local open hole feature is modelled using 3D solid elements (C3D8R) with one element per ply in the thickness direction. Further circular partitions are created concentric to the hole boundary near the region of stress concentration. The average mesh size is 1 mm outside these partitions and 0.5 mm within these partitions. In this study, we do not apply failure criteria, as our primary aim is to maximise the prediction accuracy of the 3D stresses which feed into the criteria. The error in failure index prediction will therefore scale depending on the form of the failure criterion chosen. Non-linear geometry effects are turned off. Details of the FE modelling methodology of the C-spar and open hole feature are shown in Fig. 7.

The number of plies is varied between 8 and 80. The hole radius is varied between 1 mm and 4 mm, the length and width of the local model is accordingly set as 32 mm. This allows the local model to fit within the C-spar flanges. It also allows the boundaries of the local model to exist at least 3 times the diameter away from the boundary of the largest possible hole. Maximising this distance is important with respect to Saint Venant's principle, for the submodelling process to be valid (De Saint-Venant, 1855). This distance is also informed by composite design guidelines which require holes to be at least 1.5–4 times their diameter away from other features to avoid interaction effect (Abbot, 2017). The hole radius forms the feature geometry parameter in the design of experiment and is represented simply by a scalar value.

3. Results and discussion

3.1. Effect of sample size on the design of experiment

Fig. 8 shows the sampled stacking sequences in the lamination parameter space. To construct feasible regions, we use Monte Carlo methods to generate 1000 feasible laminates and draw a convex hull around their positions. In Fig. 9 we evaluate the effect of maximin on average spacing and distribution between samples. This is shown in comparison to a random sampling strategy, and a theoretically worse sampling alternative as determined by the minimin algorithm, whereby we minimize this minimum distance between samples.

It can be seen from Fig. 8 that the samples seem well distributed in the feasible regions of the lamination parameter space. There are no signs of clustering or areas in which samples are consistently missing, apart from on the boundaries of the feasible regions. However, in our study, we are more concerned with the general prediction of behaviour and therefore have no preference for these boundary situations.

From Fig. 9(a) we confirm that the maximin algorithm results in increased average spacing. The average spacing with maximin slightly decreases with an increasing number of samples. This is expected due to the reduced space between more samples in the same feasible region. However, with an increasing number of samples, the average spacing with minimin increases. This counterintuitive effect may be explained using findings from Fig. 9(b) whereby it is shown that minimin results in a higher density of points with low spacing than maximin. The maximin criterion avoids the creation of clusters and therefore improves the distribution of samples.

3.2. Boundary condition homogenisation study

We perform a study to investigate our proposed boundary condition homogenisation method. We set up a 2D problem consisting of a rectangular steel ($E = 110GPa$, $\upsilon = 0.3$) plate with a circular hole (see Fig. 10(a)). This plate is fixed in each displacement degree of freedom along each edge, apart from one edge where it is loaded only on the x-axis. The baseline reference loading is parabolic. We use standard interpolation to generate loadings for various orders of model reduction. For example, a 2nd order model reduction results in the equivalent case of using elements of 16 mm length. According to our homogenisation method, we scale these interpolated displacements to result in equivalent work along this edge.

The effect of the order of model reduction for both interpolation and work-equivalent homogenisation on the error in stress predictions as compared to the reference loading is shown in Fig. 10(b-c). In the former, we plot the stress error at varying distances from the loaded edge, along the x-axis running through the centre of the hole. In the latter, we visualize the entire stress error field and mark the equivalent element length from the loaded edge with a white line. In Fig. 10(d) we evaluate the effect of moving the hole closer to the loaded edge, and in Fig. 10(e) we evaluate the effect of changing the hole radius.

Firstly, it can be seen from Fig. 10(b-e) that, in all cases, interpolation results in a reduced error in stress to the reference loading at the loaded edge. However, for a given order of model reduction, the work equivalent homogenisation method results in a lower error at a suitable distance away from the loaded edge. This finding supports Saint Venant's theory. Submodelling and model order reduction based on interpolation may therefore be improved by correcting displacements to ensure equivalent work on the loaded boundaries.

According to Saint Venant's theory, the stress state caused by statically equivalent force distributions, at a sufficient distance from the loading points, is approximately the same. This distance over which stress re-distribution occurs is in the order of the linear dimension of the loaded area (De Saint-Venant, 1855). In a finite element setting, this distance corresponds to the element size. For example, for non-conformal meshes (Sonnerlind, Dec. 24, 2023.), stress re-distributes after an element's length away from the loaded boundary. Similarly, we find that the distance from the loaded boundary at which stresses re-distribute is not the same for different orders of model order reduction. From Fig. 10(b-c), for example, we see that the higher the order of model order reduction, the lower this distance. The element size defines the polynomial order that is used to fit the reference loading and therefore it follows that the element size is proportional to the length required for stress redistribution.

In Fig. 10(d-e), we find that repositioning the hole closer to the loaded edge adversely affects the load redistribution. This occurs regardless of whether homogenisation or interpolation is used. For high-order model reduction this error is reduced but still significant, despite the hole boundary being more than 8 mm away from the loaded edge.

Table 1
Material properties of carbon fibre epoxy pre-preg (Kevin O'brien and R. Krueger, 2001).

E11 (GPa)	E22(GPa)	E33(GPa)	ν12	ν13	ν23	G12(GPa)	G13(GPa)	G23(GPa)
161	11.4	11.4	0.32	0.32	0.43	5.17	5.17	3.98

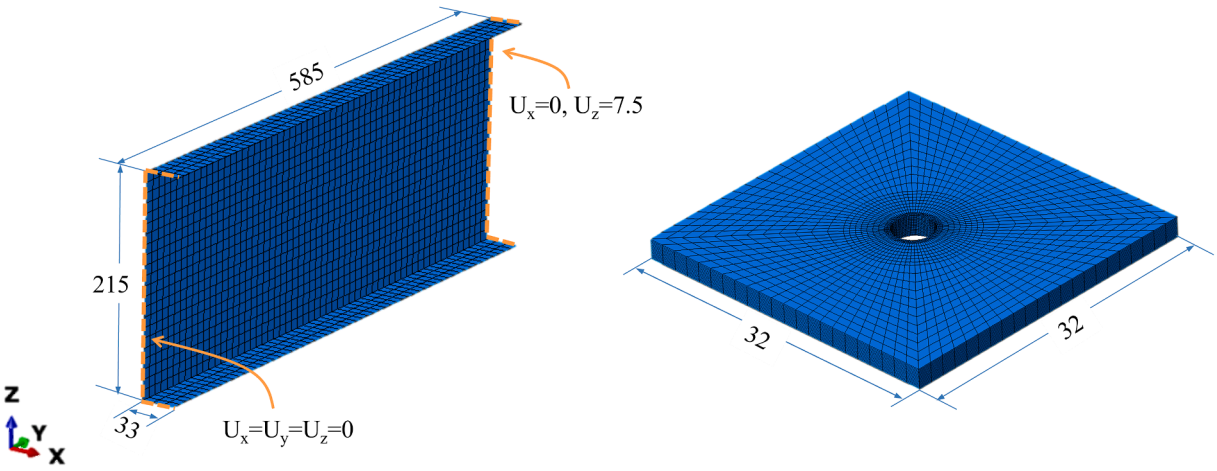

Fig. 7. Modelling details of global C-spar model (left) and local open hole model (right).

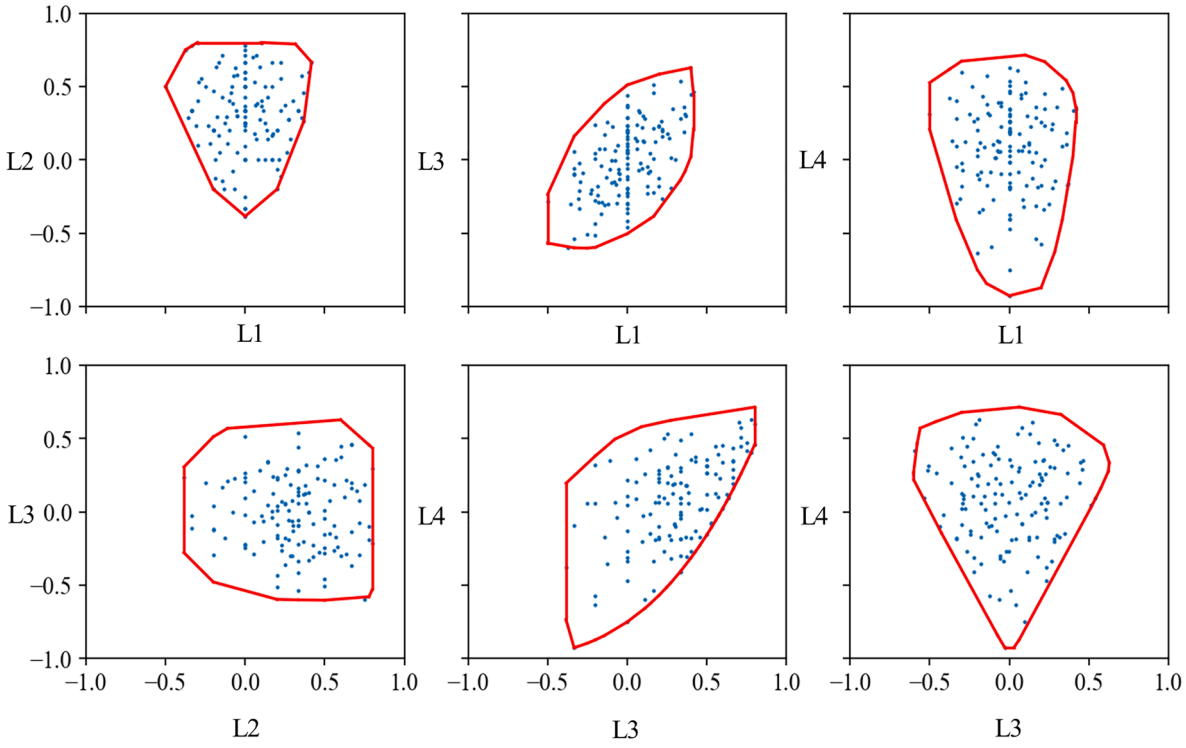

Fig. 8. Lamination parameter space: distribution of laminates used in study plotted within their feasible regions.

This indicates that the presence of the hole close to the loaded edge either reduces the redistribution rate of stresses, or that the stresses were not completely re-distributed at this distance, and the boundaries of the open hole magnify this error. Halving the hole radius provides another 2 mm for the stresses to redistribute and reduces the stress error at the hole boundary.

For open hole tensile specimens and features such as bolted joints, the stress at or near the boundary is of critical importance for failure predictions. Therefore, it is advised that a safety factor is given to the expected length of stress re-distribution to account for the presence of the local feature boundary. This can then inform the appropriate order of model reduction. In our study, for example, the minimum distance between the hole boundary and the local model edge is 12 mm. Therefore, a safety factor of 2 would require an element edge length of 6 mm, so at least a 6th-order model reduction would be advised.

3.3. Volume averaged stress study

To gain an intuition of the volume averaged stress method we load the 3D local model with various displacements as shown in Fig. 11(a). We fix the displacement degrees of freedom on all boundaries, except the x displacement degree of freedom on one loaded boundary. We apply a uniform tensile loading across this boundary and a uniform compressive loading. For the uniform tensile loading case, we plot the effect of varying the distance to the hole boundary over which we volume average on volume averaged stresses (see Fig. 11(b)). In Fig. 11(c), we plot the stress component in the x-direction at varying distances from the hole boundary in the net section and loading planes, for a 0° ply. The net section plane is perpendicular to the primary loading direction and the loading plane is defined as parallel to the primary loading direction. Finally, in Fig. 11(d), we plot a volume averaged stress component for all 6000 plies across all sampled laminates as a result of a unit displacement

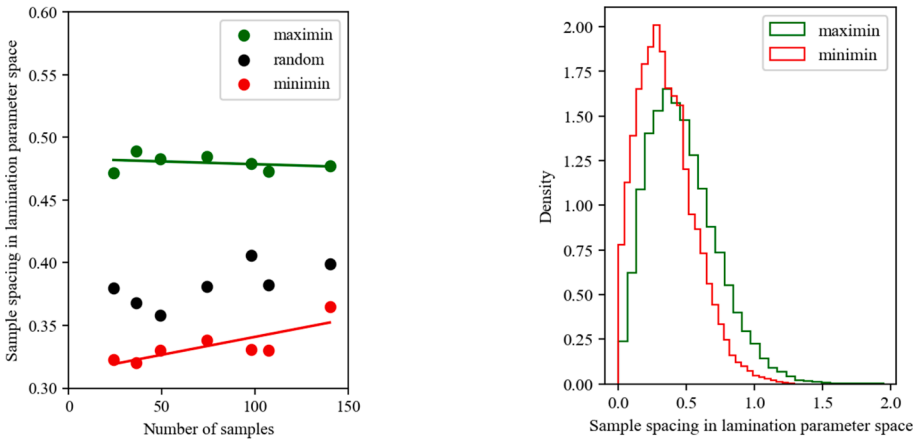

(a) Effect on average sample spacing (b) Effect on sampling

Fig. 9. Effect of maximin on sampling in the lamination parameter space.

at a given degree of freedom.

The volume averaged stresses due to tensile loading are found to be equal to the opposite due to compressive loading. Stress re-distribution effects from volume averaging do not affect linear superposition. Therefore, even though it is advised to use 6th-order homogenisation for the geometry in our study, we can simplify the degrees of freedom to 2nd-order homogenisation when testing our ML models in the next section.

Increasing the distance to the hole boundary in the net section plane should reduce averaged stresses (see Fig. 11(c)). Conversely, increasing the distance to the hole boundary in the loading plane should increase averaged stresses (see Fig. 11(c)). When increasing the distance to the hole boundary that we use to volume average, the stresses in the 0° plies increase (see Fig. 11(b)). Therefore, the increase in stress in the loading plane is offsetting the decrease in stress in the net section plane.

In this case, the stresses in the loading plane have a dominating influence on the volume averaged stress. For a given loading, the important stresses in the net section plane are masked by the effects of the stresses in the loading plane. This interaction means that volume averaging has limited benefit in use towards a failure criterion, especially for bolted joints where bearing-bypass interactions at orthogonal planes occur. A potential improvement would be to restrict volume averaging to areas where stress behaviour is similar throughout, such as restricted angular regions in net section and loading planes.

Despite recognizing these limitations, volume averaging still provides non-trivial 3D stress values for the ML model to predict. As visible from Fig. 11(d), there is still a large variation between volume averaged stresses in plies of the same angle. Therefore, volume averaging is useful to develop the proof of concept for our ML methodology.

3.4. *Effect of neural network customisations*

In Fig. 12 we compare the effect of using various neural network architectures on the training and validation error of the ML model. This is done for varying numbers of neurons in the network. Training error indicates the capability of the neural network to learn from data it has seen, and validation error indicates the network's capability to generalize to data it has not seen.

LSTM networks show reduced error metrics for a given number of neurons compared to RNN networks. Further, unlike for RNNs, increasing the number of neurons consistently reduces the training error indicating that there is still room for the network to learn beyond the number of neurons tested. However, validation errors remain at a similar level. This indicates that there is a large amount of overfitting that increases with the number of neurons.

Dropout is a common technique used to address overfitting. In this case, recurrent dropout is used, whereby 20 % of connections between hidden states in the neural network are dropped. Validation errors are reduced, however they remain at a similar level regardless of increasing the number of neurons. This suggests that dropout may need to increase as the number of neurons in the network increases.

We also compare the effect of stacking two LSTM layers. With an increasing number of neurons, the training error reduces further than without stacking. Stacking adds an abstraction layer which may be useful to better learn the interaction of hole radius and laminate stacking sequence. However, stacking results in a higher degree of overfitting and therefore increased dropout may be necessary to fully benefit from this architecture.

The use of a bidirectional wrapper around the LSTM doubles the number of neurons. In this case, an extra layer of neurons in the opposite direction to the forward LSTM layer is used to inform predictions at the beginning of the sequence with values at the end of the sequence. As with stacking, the use of bidirectionality is of benefit beyond 80 neurons. In this case, however, both training and validation errors are reduced and there is less overfitting.

We combine the benefits of bidirectionality, stacking and dropout to form a best-performing combination network. The 20 % dropout used in this case is applied between the two layers of bidirectional networks. This network outperforms the previously tested networks, in terms of training error and most importantly validation error.

3.5. *Application: Stress distribution predictions of an open hole on a composite C-spar*

In Fig. 13 we compare the predictions made by the best-performing neural network with the reference FE volume averaged stresses for a local hole in plate feature driven by the homogenized displacements from the global C-spar simulation. This is done for two cases of varying hole geometry, laminate stacking sequence and loading conditions.

In both cases, the ML model can closely predict the variation in volume averaged 3D stress fields. The ML model has higher performance for in-plane stress components, than for through-thickness stress components. This may be because there was no direct through-thickness loading applied. The ML model may therefore have difficulty in picking up the variation between these negligibly low magnitude stresses.

The ML model achieved these predictions with an average clock time of 182 ms, the equivalent FE analyses take an average of 25 s. This represents over 130 times factor of time-saving benefit. This time-saving compounds given that such features may exist in the thousands for composite structures, and would further compound for airframe level optimisation studies. The ML approach also saves time spent online on model generation, which depending on the feature and the FE analyst may take minutes or hours.

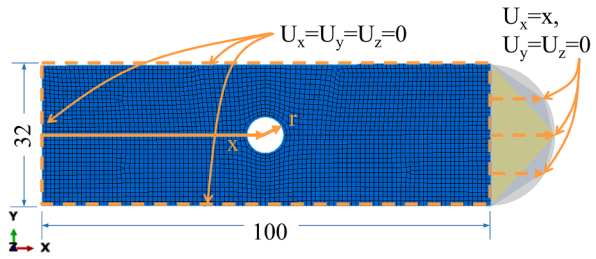

(a) FE modelling details

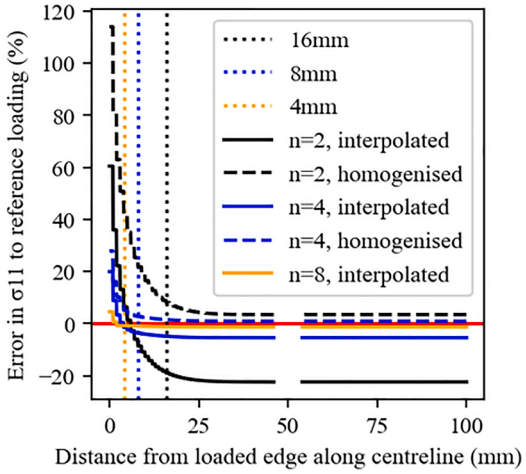

(b) Baseline errors for hole with r=2 at x=50

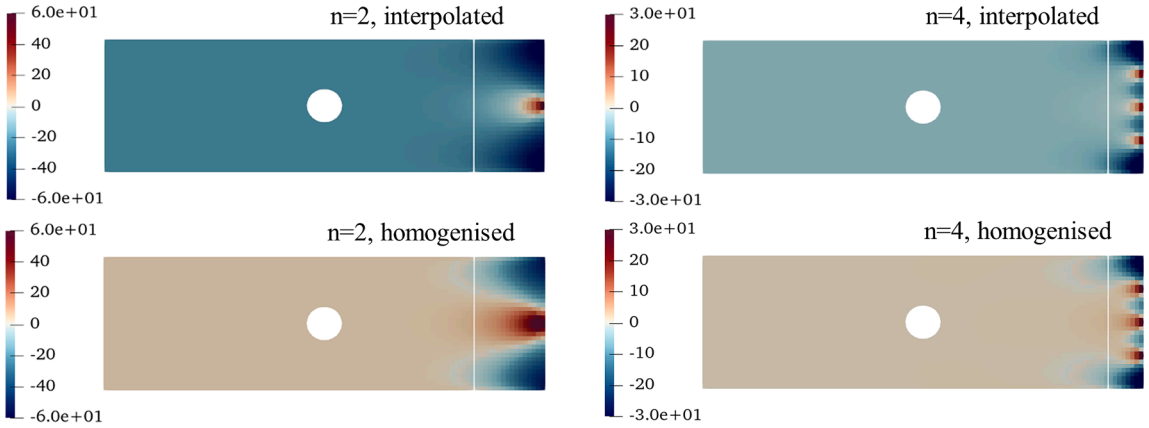

(c) Error in stress field for hole with r=2 at x=50

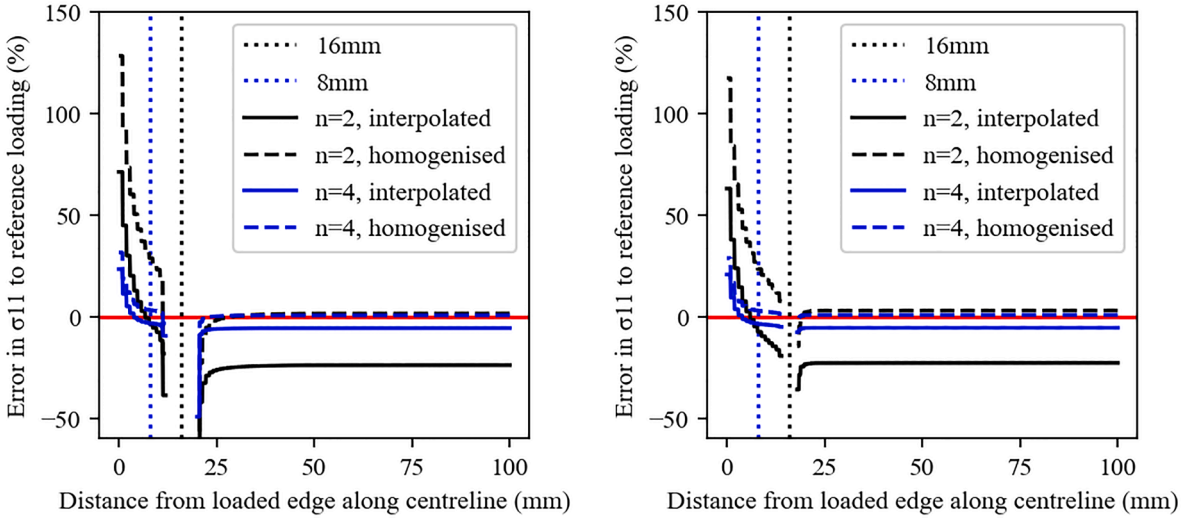

(d) Effect of moving hole to x=84

(e) Effect of reducing hole radius to r=2

Fig. 10. Boundary condition study to investigate the effect of order of interpolation and homogenisation on error in stress distributions.

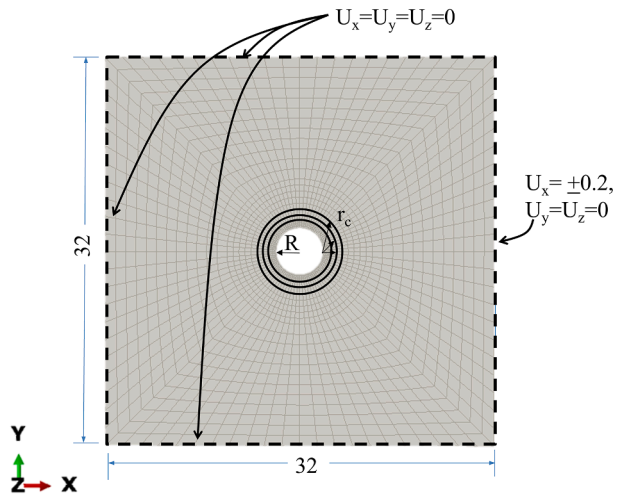

(a) FE modelling details

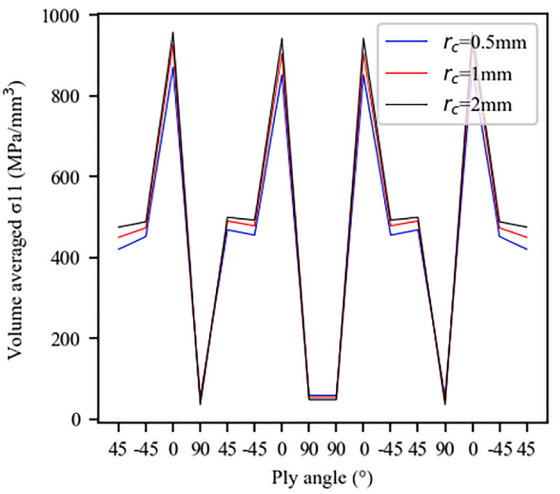

(b) Effect of distance to hole boundary

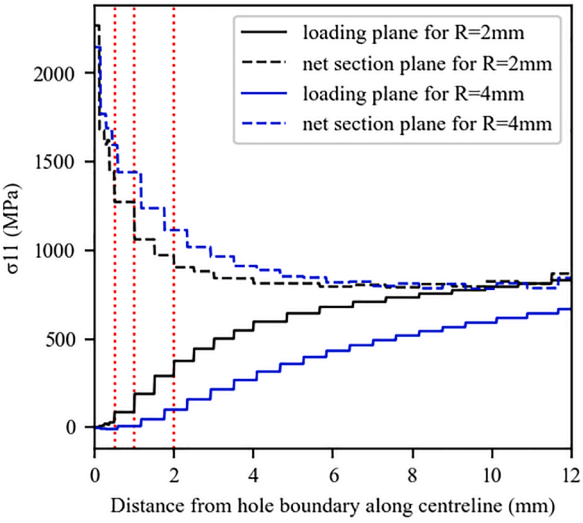

(c) stress distribution on loading and net section planes

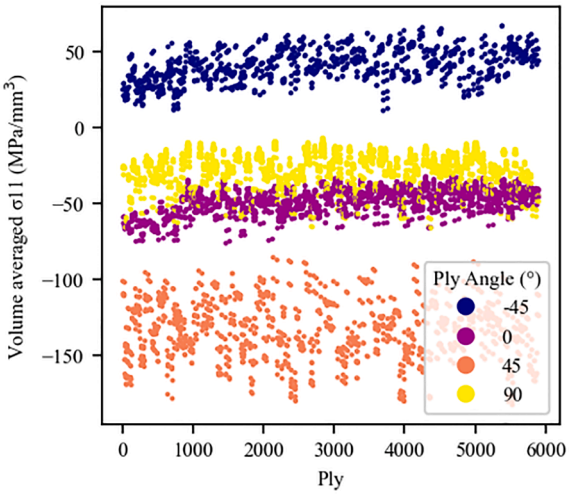

(d) Variation in volume averaged stresses

Fig. 11. Effect of ply angle and distance to hole boundary for volume averaged stress method.

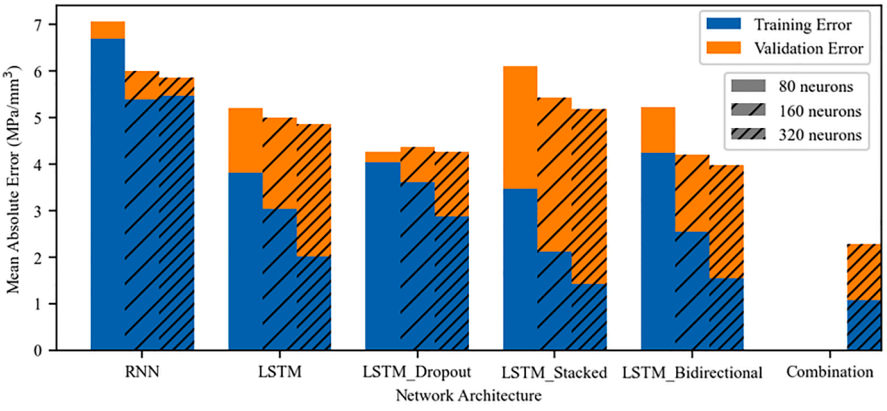

Fig. 12. Training and validation errors for various neural network architectures.

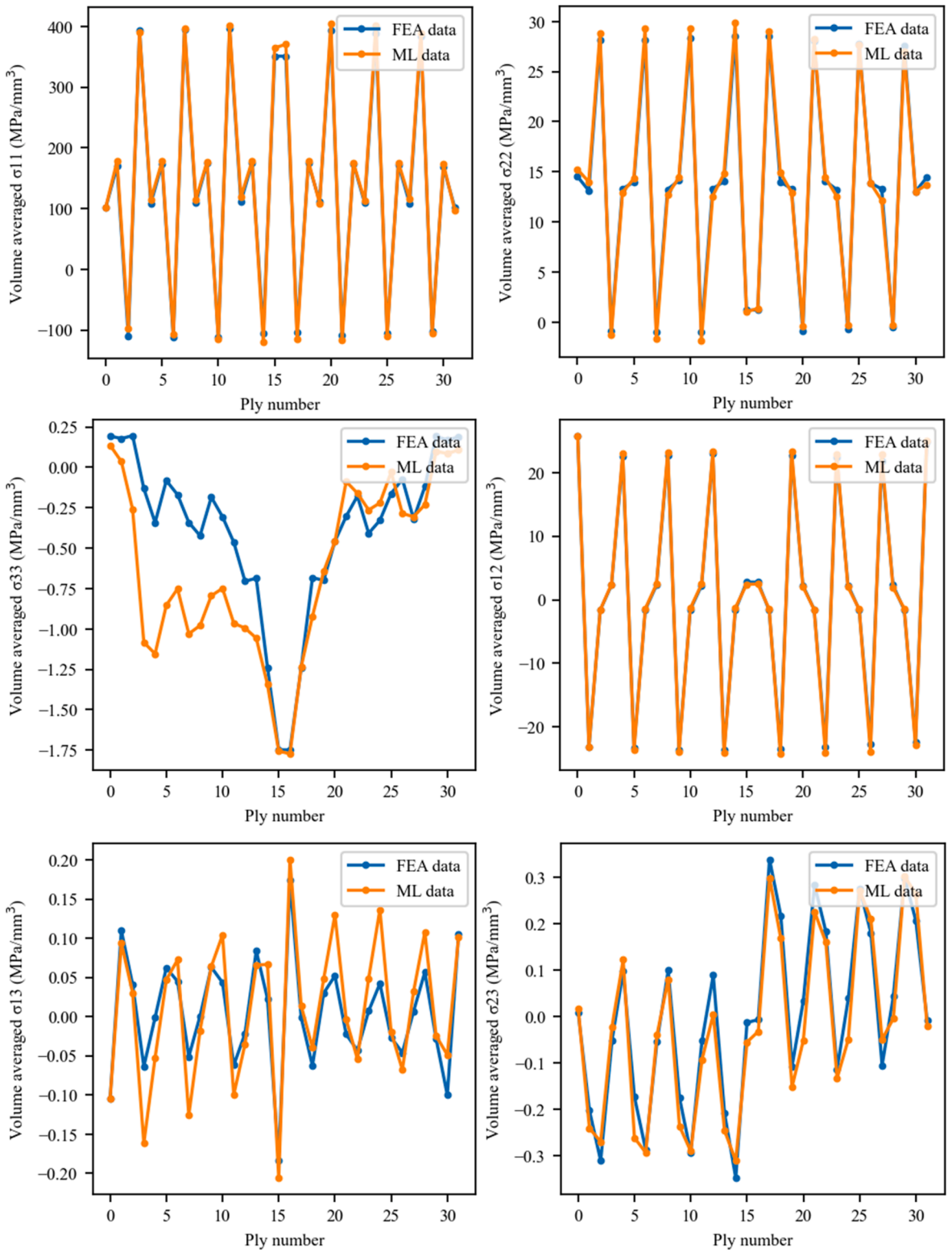

(a) $[45,-45,0,90]_{4s}$ laminate with 2mm radius hole loaded in tension on bottom flange of C-spar.

Fig. 13. ML model prediction of all volume averaged stress components compared to high-fidelity FE results for an open hole feature in a composite C-spar structure.

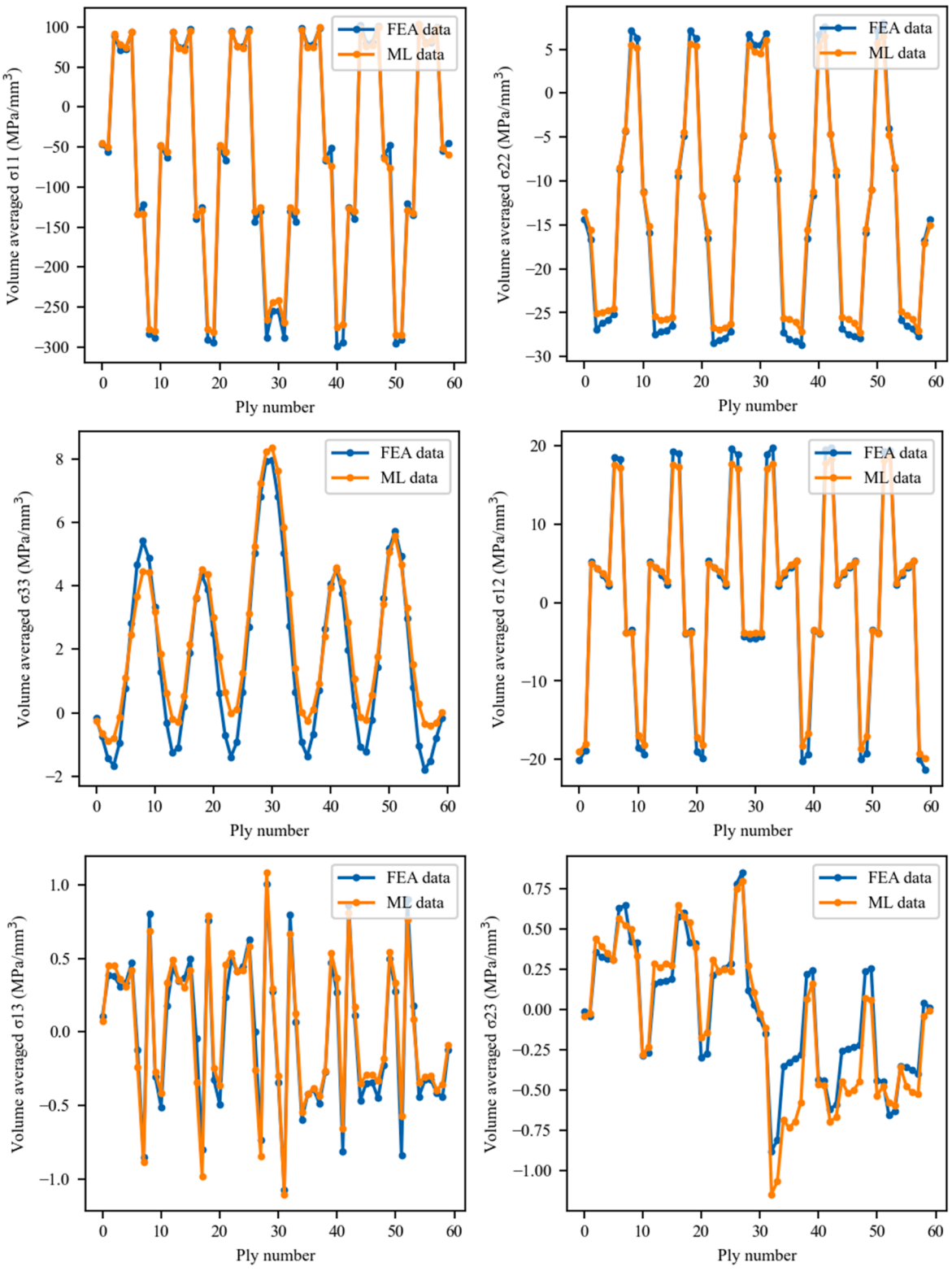

(b) $[45,45,0,0,0,0,-45,-45,90,90]_{3s}$ laminate with 4mm radius hole loaded in compression on top flange of C-spar.

Fig. 13. (*continued*).

4. Conclusions

In this work, we developed a ML assisted framework for the stress analysis of a hole in plate feature in an aerospace C-spar structure, with the following original features: a computationally efficient sampling scheme; a work-equivalent boundary condition homogenisation scheme; a volume averaged ply-by-ply stress approach; and a sequential long-short term memory neural network reformulated from a time basis to a stacking sequence basis with further bi-directionality customisation. This is the first use of machine learning within the global–local method for mesoscale ply-by-ply volume averaged stresses in the literature.

Our design of experiment is shown to result in well-distributed sampling stacking sequences in both the lamination parameter space and the ply angle space. This design of experiment operates without computationally expensive genetic algorithms, and we show that the design of experiment is of increasing value when the dataset size is reduced.

A work-equivalent homogenisation technique is developed for model order reduction of the boundary conditions. This technique results in improved stress accuracy as compared to the standard interpolation methods. However, we suggest that the order of homogenisation be such that the resultant element edge length between reduced order boundary nodes be less than the distance to the feature boundaries, by a safety factor. This safety factor must be determined on a case-by-case basis depending on the local feature in question.

Volume averaging of stress components within a given distance to the hole boundary allows a single vector to be predicted per ply. Although we have shown limitations of such volume averaging for failure criterion applications, the volume averaged stresses still reflect non-trivial differences in 3D stress distributions that can be used to determine failure in reference to a known distribution of volume averaged stresses occurring at failure.

Our best-performing ML model comprises a LSTM network which is shown in this study to be beneficial over a RNN due to the consideration of long-range effects in stacking sequence, which may inform stiffness and therefore stress predictions. A bi-directional wrapper is shown to improve learning for the symmetric laminates used in this study.

Our overall ML framework can predict 3D stress distributions of the laminate to a satisfactory accuracy and with a significant time-saving benefit over high-fidelity FE methods. This approach therefore has the potential to save significant time in predictive virtual testing of repetitive features in large composite structures.

Declaration of competing interest

The authors declare that they have no known competing financial interests or personal relationships that could have appeared to influence the work reported in this paper.

Data availability

Data will be made available on request.

Acknowledgements

This study was supported by funding from the Department of Aeronautics, Imperial College London. The second author acknowledges funding from EPSRC project EP/W022508/1. The authors express their gratitude and remembrance of the late Professor Lorenzo Iannucci for his various contributions to this research.

References

M. Abadi *et al.*, "TensorFlow: A System for Large-Scale Machine Learning TensorFlow: A system for large-scale machine learning," 2016.

R. Abbot, *Analysis and Design of Composite and Metallic Flight Vehicle Structures, vol. 2nd Edition. 2017*.

Akterskaia, M., Jansen, E., Hallett, S.R., Weaver, P.M., Rolfes, R., 2019. Progressive failure analysis using global-local coupling including intralaminar failure and debonding. AIAA J. 57 (7), 3078–3089. https://doi.org/10.2514/1.J057677.

Albazzan, M.A., Harik, R., Tatting, B.F., Gürdal, Z., Feb. 2019. Efficient design optimization of nonconventional laminated composites using lamination parameters: A state of the art. Compos Struct 209, 362–374. https://doi.org/10.1016/J.COMPSTRUCT.2018.10.095.

Cessna Citation Mustang Dimensions - FlyRadius." Accessed: Dec. 24, 2023. [Online]. Available: https://www.flyradius.com/cessna-citation-mustang/dimensions.

F. Chollet, "Keras." Accessed: Dec. 15, 2023. [Online]. Available: https://keras.io.

R. Creemers, J. Botma, and B. J. G. Eussen, "Conceptual design for the retrofit of a fighter type wing by a composite skin in the NTP wing composites research programme," 2009.

Dassault Systemes, "Abaqus Standard." Accessed: Dec. 15, 2023. [Online]. Available: https://www.3ds.com/.

B. De Saint-Venant, "Mem. Acad. Sci. Savants etrangers," vol. 14, pp. 233–560, 1855.

Fan, W., Yin, L., Xu, Z., Zhang, Z., 2023. Two-stage surrogate-based optimization of a vehicle composite subframe with modified fast flexible space-filling designs. Mech. Adv. Mater. Struct. 30 (4), 724–737. https://doi.org/10.1080/15376494.2021.2023916.

Aurélien Géron, *Hands-on machine learning with Scikit-Learn, Keras and TensorFlow: concepts, tools, and techniques to build intelligent systems*. 2019.

Global Market Forecast | Airbus." Accessed: Dec. 24, 2023. [Online]. Available: https://www.airbus.com/en/products-services/commercial-aircraft/market/global-market-forecast.

IATA - Fly Net Zero." Accessed: Dec. 24, 2023. [Online]. Available: https://www.iata.org/en/programs/environment/flynetzero/.

Joseph, V.R., Gul, E., Ba, S., Jun. 2015. Maximum projection designs for computer experiments. Biometrika 102 (2), 371–380. https://doi.org/10.1093/BIOMET/ASV002.

T. Kevin O'brien and R. Krueger, "Analysis of Ninety Degree Flexure Tests for Characterization of Composite Transverse Tensile Strength," 2001, Accessed: Dec. 15, 2023. [Online]. Available: http://www.sti.nasa.gov.

Krokos, V., Bui Xuan, V., Bordas, S.P.A., Young, P., Kerfriden, P., Mar. 2022. A Bayesian multiscale CNN framework to predict local stress fields in structures with microscale features. Comput. Mech. 69 (3), 733–766. https://doi.org/10.1007/S00466-021-02112-3/FIGURES/42.

Krueger, R., O'Brien, T.K., Jan. 2001. A shell/3D modeling technique for the analysis of delaminated composite laminates. Compos. Appl. Sci. Manuf. 32 (1), 25–44. https://doi.org/10.1016/S1359-835X(00)00133-0.

Le, B.A., Yvonnet, J., He, Q.C., Dec. 2015. Computational homogenization of nonlinear elastic materials using neural networks. Int. J. Numer. Methods Eng. 104 (12), 1061–1084. https://doi.org/10.1002/NME.4953.

Logarzo, H.J., Capuano, G., Rimoli, J.J., Jan. 2021. Smart constitutive laws: Inelastic homogenization through machine learning. Comput. Methods Appl. Mech. Eng. 373, 113482 https://doi.org/10.1016/J.CMA.2020.113482.

Nagaraj, M.H., Petrolo, M., Carrera, E., Dec. 2021. A global–local approach for progressive damage analysis of fiber-reinforced composite laminates. Thin-Walled Struct. 169, 108343 https://doi.org/10.1016/J.TWS.2021.108343.

Niu, C., 1992. Composite Airframe Structures Practical Design Information and Data. Hong Kong Conmilit Press limited.

Ostergaard, M.G., Ibbotson, A.R., Le Roux, O., Prior, A.M., Sep. 2011. Virtual testing of aircraft structures. CEAS Aeronaut. J. 1 (1–4), 83–103. https://doi.org/10.1007/S13272-011-0004-X.

Reille, A., et al., 2021. Learning data-driven reduced elastic and inelastic models of spot-welded patches. Mech. Ind. 22, 32. https://doi.org/10.1051/MECA/2021031.

RStudio Team, 2020. RStudio: Integrated Development for R. Boston.

H. Sonnerlind, "Applying and Interpreting Saint-Venant's Principle | COMSOL Blog." Accessed: Dec. 24, 2023. [Online]. Available: https://www.comsol.com/blogs/applying-and-interpreting-saint-venants-principle/.

Sun, Z., Lei, Z., Zou, J., Bai, R., Jiang, H., Yan, C., Sep. 2021. Prediction of failure behavior of composite hat-stiffened panels under in-plane shear using artificial neural network. Compos Struct 272, 114238. https://doi.org/10.1016/J.COMPSTRUCT.2021.114238.

SwiftComp for Efficient Modeling of Composites | AnalySwift. Accessed: Dec. 24, 2023. [Online]. Available: https://analyswift.com/swiftcomp-vamuch-micromechanics-modeling-of-heterogeneous-materials-2/.

J. M. Whitney and R. J. Nuismer, "Stress Fracture Criteria for Laminated Composites Containing Stress Concentrations," *https://doi.org/10.1177/002199837400800303*, vol. 8, no. 3, pp. 253–265, Jul. 1974, doi: 10.1177/002199837400800303.

Xu, R., et al., May 2020. Data-driven multiscale finite element method: From concurrence to separation. Comput. Methods Appl. Mech. Eng. 363, 112893 https://doi.org/10.1016/J.CMA.2020.112893.

Zou, X., Yan, S., Ilkhani, M.R., Brown, L., Jones, A., Hamadi, M., Mar. 2021. An Abaqus plugin for efficient damage initiation hotspot identification in large-scale composite structures with repeated features. Adv. Eng. Softw. 153, 102964 https://doi.org/10.1016/J.ADVENGSOFT.2020.102964.